Mitochondria- and ER-associated actin are required for mitochondrial fusion

Priya Gatti[1,2,3], Cara Schiavon[4,5], Uri Manor[4,6#], Marc Germain[1,2,3#]

[1]Groupe de Recherche en Signalisation Cellulaire and Département de Biologie Médicale, Université du Québec à Trois-Rivières, Trois-Rivières, Québec, Canada

[2]Centre d'Excellence en Recherche sur les Maladies Orphelines - Fondation Courtois, Université du Québec à Montréal, Montréal, Québec, Canada

[3]Réseau Intersectoriel de Recherche en Santé de l'Université du Québec (RISUQ)

[4]Waitt Advanced Biophotonics Center, Salk Institute for Biological Studies, La Jolla, CA, United States.

[5]Molecular and Cell Biology Laboratory, Salk Institute for Biological Studies, La Jolla, CA, United States

[6]Department of Cell and Developmental Biology, School of Biological Sciences, University of California, San Diego, La Jolla, CA, United States.

Correspondence:

Uri Manor: urmanor@ucsd.edu

Marc Germain: marc.germain1@uqtr.ca

Abstract

Mitochondria play a crucial role in the regulation of cellular metabolism and signalling. Mitochondrial activity is modulated by the processes of mitochondrial fission and fusion, which are required to properly balance respiratory and metabolic functions, transfer material between mitochondria, and remove damaged or defective mitochondria. Mitochondrial fission occurs at sites of contact between the endoplasmic reticulum (ER) and mitochondria, and is dependent on the formation of mitochondria- and ER-associated actin filaments that drive the recruitment and activation of the fission GTPase DRP1. On the other hand, the role of mitochondria- and ER-associated actin filaments in mitochondrial fusion remains unknown. Here we show that preventing the formation of actin filaments on either mitochondria or the ER using organelle-targeted Disassembly-promoting, encodable Actin tools (DeActs) blocks both mitochondrial fission and fusion. We show that fusion but not fission is dependent on Arp2/3, and both fission and fusion are dependent on INF2 formin-dependent actin polymerization. Together, our work introduces a novel method for perturbing organelle-associated actin filaments, and demonstrates a previously unknown role for mitochondria- and ER-associated actin in mitochondrial fusion.

Introduction:

Mitochondria play a crucial role in the regulation of cellular metabolism and signalling, thereby controlling key cellular processes including apoptosis, cell fate decisions, and inflammation. These activities are regulated by mitochondrial dynamics, the process of fusion and fission which controls mitochondrial shape, size, and function. Mitochondrial dynamics allows for the exchange of components, such as lipids and proteins, and the removal of damaged or defective mitochondria, maintaining the overall function and quality of mitochondria (Chandel, 2015, Chen et al., 2003, Shirihai et al., 2015, Tan and Finkel, 2020, Detmer and Chan, 2007).

Mitochondrial dynamics are controlled by a family of dynamin-related GTPases: mitochondrial fission requires Dynamin Related Protein 1 (DRP1), while mitochondrial fusion depends on mitofusins (MFN1 and MFN2) for the fusion of the outer membrane and OPA1 for the fusion of the inner membrane. In addition to this core machinery, mitochondrial fission requires specific contacts with the endoplasmic reticulum (ER), which marks fission sites (Friedman et al., 2011). These ER-mitochondria contact sites then work as platforms to recruit the fission machinery. One of the key events occurring at ER-mitochondria contact sites during fission is the recruitment of Inverted Formin 2 (INF2). This actin-polymerizing protein catalyzes the elongation of actin filaments at ER-mitochondria contacts (Korobova et al., 2013, Schiavon et al., 2020). These actin filaments are subsequently used by non-muscle myosin II to constrict the mitochondrion (Korobova et al., 2014, Yang and Svitkina, 2019). This partial constriction then allows the recruitment of the fission protein DRP1, followed by DRP1-dependent scission of the mitochondrion. Consistent with this, inhibiting actin polymerization, myosin II activity, or INF2 decreases Drp1 oligomerization on mitochondria, suggesting that actin and myosin are involved in the recruitment and activation of Drp1 (Li et al., 2015, Hatch et al., 2014, Ji et al., 2015, Liu et al., 2021).

Regulation of mitochondrial fusion is less well understood. Recent studies have demonstrated that the ER is present not only at fission sites but also at fusion sites (Abrisch et al., 2020) where it was suggested to accelerate the fusion process (Guo et al., 2018). Consistent with this, loss of ER-mitochondria contact sites decreases the number of fusion and fission events (Nguyen and Voeltz, 2022). Nevertheless, the exact role of the ER in mitochondrial fusion remains to be elucidated. One possibility is that it acts as a platform to recruit the fusion machinery, similarly to what occurs during fission (Friedman et al., 2011, Korobova et al., 2013, Abrisch et al., 2020).

Previous research supports important roles for mitochondria-associated actin aside from its role in mitochondrial fission. This includes mitochondria quality control (Fung et al., 2022) and the regulation mitochondrial movements (Boldogh et al., 2005, Doniwa et al., 2007, Fernandez Casafuz et al., 2023, Lopez-Domenech et al., 2018). Similarly, actin plays an important role in recruiting and activating dynamin family GTPases to various cell compartments (Gu et al., 2014, Gu et al., 2010). As the ER likely acts as a platform to recruit the machinery for both mitochondrial fission and fusion, and since mitochondria- and ER-associated actin plays a crucial role in GTPase-mediated mitochondrial fission, we hypothesize that mitochondria- and ER-associated actin is also involved in GTPase-mediated mitochondrial fusion.

Here, we address the role of actin in the regulation of mitochondrial fusion. Using fluorescent protein-tagged mitochondria- and ER-targeted actin nanobodies, we demonstrate that actin marks sites of mitochondrial fusion. Importantly, inhibiting actin polymerization specifically on mitochondria or the ER disrupts mitochondrial fusion. In addition, inhibiting the actin nucleation protein complex Arp2/3 or ER-anchored INF2 similarly prevents mitochondrial fusion. Our work also reveals two mechanistically distinct types of fusion events (tip-to-tip vs. tip-to-side) based on their requirement for mitochondrial actin. Therefore, our data demonstrates a key organizational and regulatory role of mitochondria- and ER-associated actin in mitochondrial fusion.

Actin accumulates at sites of mitochondrial fusion

To monitor the presence of actin at the site of mitochondrial fusion, we used GFP-tagged actin nanobodies (termed Actin Chromobodies (AC)) targeted to the outer mitochondrial membrane with the c-terminal transmembrane domain of Fis1 (AC-mito) (Schiavon et al., 2020). AC-mito moves freely within the mitochondrial membrane giving a diffused signal. However, when the AC probe binds to mitochondria-associated actin, it becomes immobilised, resulting in a higher intensity signal at the actin-associated site. We have previously used these probes to show the accumulation of actin at sites of mitochondrial fission (Schiavon et al., 2020).

We transfected primary human fibroblasts with AC-mito and a control mCherry construct targeted to mitochondria with the same Fis1 transmembrane domain as AC-mito (mCherry-mito) to label mitochondria (Figure 1A) and imaged them live with confocal microscopy. We then analysed the presence of the AC probe at the site of mitochondrial fission and fusion. Consistent with previous studies, we observed AC-mito accumulation at fission sites (Figure 1B), validating the approach. Importantly, we also observed AC-mito accumulation at fusion sites in most fusion events (Figure 1A-B, video 1). To confirm AC-mito accumulation at fusion and fission sites, we measured its specific enrichment relative to adjacent mitochondria. We observed a 2-fold increase in enrichment of AC-mito signal at fusion (Fig.1C) and fission (Fig. 1D) events, which was absent when measured using the mCherry-mito signal which consistently spreads evenly across mitochondrial surfaces (Fig. 1C-D). Our data thus clearly demonstrates that AC-mito is enriched at sites of mitochondrial fusion, indicating the presence of mitochondria-associated actin at these sites.

As sites of mitochondrial fusion are associated with actin, and fusion is mediated by the mitochondrial outer membrane dynamin-related GTPase MFNs, we asked whether promoting MFN-mediated fusion is sufficient to drive actin polymerization on mitochondria. To stimulate fusion, we overexpressed MFN1 in our primary fibroblasts. As predicted, MFN1 overexpression leads to clustering and fusion of mitochondria (Legros et al., 2002, Huang et al., 2007) (Figure 1E). These changes were accompanied by a large increase in AC-mito signal (Figure 1E-F). Thus, promoting MFN1-mediated mitochondrial fusion is sufficient to stimulate actin association with mitochondria.

Mitochondrial fusion occurs in two distinct ways: tip-to-tip fusion, where the end of one mitochondrion fuses with the end of another, and tip-to-side fusion, where the end of a mitochondrion fuses at the side of another mitochondrion (Nguyen and Voeltz, 2022) (Figure 2A). Notably, our data revealed that 75% of fusion events involved tip-to-side fusion (Figure 2B). Interestingly, actin was much more likely to

be present at tip-to-side events (88%) than end-to end events (50%) (Fig. 2C), suggesting that actin predominantly favors tip-to-side fusion. We also observed that in most fusion events, one mitochondrion remains immobile while the other is mobile (Figure 2D, “Still”). This was however not the case for tip-to-tip fusions, where both mitochondria involved were usually mobile (Figure 2E).

Our subsequent objective was to identify which of the two fusing mitochondria recruited actin. Since most fusion events involved one immobile mitochondrion, we selected this subset for further analysis. We referred to the immobile mitochondrion as the "receiving mitochondrion" and the moving one as the "fusing mitochondrion". By examining the AC-mito enrichment at the receiving and fusing ends of the mitochondrion, we discovered that actin is present to a greater extent on the immobilized receiving mitochondrion than on the fusing mitochondrion and that the AC-mito signal persists until the end of the fusion event (Figure 2F). Altogether, our findings indicate mitochondria-associated actin acts as a marker for the sites of mitochondrial fusion.

Actin-associated mitochondrial fusion sites recruit the endoplasmic reticulum (ER)

During mitochondrial fission, the ER acts as a platform to recruit actin-regulatory proteins (INF2) and actin-binding motor proteins (non-muscle myosin II) leading to mitochondrial constriction and DRP1-mediated scission of the mitochondrion (Friedman et al., 2011, Ji et al., 2015, Korobova et al., 2014, Korobova et al., 2013, Li et al., 2015, Manor et al., 2015). To measure the presence of ER at fusion sites, we transfected primary fibroblasts with mCherry targeted to the ER using the c-terminal domain of cytochrome b5 (mCherry-ER) and CCO-IRES (EGFP tagged inner mitochondrial membrane marker), imaged live with confocal microscopy. Consistent with previous reports, most fusion and fission events were associated with the presence of ER (Figure 3A). We then tested whether ER-associated actin was also recruited at mitochondrial fusion sites. To specifically determine if ER-associated actin was present at fusion sites we used our previously reported variation of the AC probe that was targeted to the ER using the c-terminal domain of cytochrome b5 (AC-ER) (Schiavon et al., 2020). We simultaneously transfected cells with AC-ER and mCherry-mito and assessed the recruitment of AC-ER at fusion sites (Figure 3B). Similar to AC-mito, most fusion and fission events were positive for AC-ER (Figure 3C). The enrichment of AC-ER was confirmed at fusion (Figure 3D) and fission sites (Figure 3E) as for AC-mito. Like AC-mito, most receiving mitochondria were AC-ER-positive, while fusing mitochondria were less likely to show AC-ER signal (Figure 3F). Therefore,

our results indicate that both mitochondria- and ER-associated actin are present at mitochondrial fusion sites.

During mitochondrial fission, mitochondria-associated actin accumulates first at the fission site, followed by ER-associated actin filaments prior to fission (Schiavon et al., 2020). We thus investigated the temporal relationship between the recruitment of AC-ER and AC-mito at fusion sites. To determine when mitochondria- and ER-associated actin filaments are recruited to the mitochondrial fusion site, cells were co-transfected with AC-Mito, a halo-tagged version of AC-ER, and mCherry-mito. We then measured ER- and mitochondria-associated actin recruitment relative to fusion events. Similar to what we observed for mitochondrial fission, we found that AC-mito was recruited first to the future fusion site, followed by AC-ER (Figure 3G, fusion occurs at timepoint 0). Specifically, AC-ER was recruited at the fusion site at an average of 100 seconds after AC-mito (Fig. 3H), suggesting that recruitment of actin on mitochondria, not the ER, is the primary event for mitochondrial fusion.

Mitochondrial actin is required for fusion

As our results show that actin is associated with mitochondrial fusion, we then asked whether it was required for fusion. Actin depolymerizing drugs impact many subcellular processes and signaling pathways, making it difficult to distinguish primary from secondary effects. Thus, the ability to selective remove actin from subcellular compartments of interest would be enormously valuable for the cell biology research community. To address this gap and selectively remove actin from mitochondria, we modified a recently described Disassembly-promoting, encodable Actin tool (DeAct), a ~120 amino acid domain of the actin-regulating protein Gelsolin (Gelsolin Segment 1 - aa 53-176 – GS1) that sequesters actin monomers (Harterink et al.). To specifically target GS1 to mitochondria or the ER, we fused it to the c-terminal transmembrane domain of Fis1 (DeAct-mito) or cytochrome b5 (DeAct-ER).

After confirming the proper localisation of the constructs (Supp. Figure 1A-B), we first determined if organelle-targeted DeAct prevented actin accumulation on mitochondria by co-transfecting DeActs-mScarlet (mito or ER) with AC-mito or AC-ER. Consistent with the ability of DeAct to locally disrupt actin filaments, DeAct-mito significantly decreased AC-Mito signal intensity (Figure 4A-B), while AC-ER showed a steep decline when transfected with DeAct-ER (Figure 4C, Sup. Figure 2). We also tested whether the organelle-targeted DeActs specifically affected their target organelle. DeAct-mito did not significantly affect AC-ER signal, highlighting the selectivity of the probe (Figure 4A-C). In

contrast, DeAct-ER was also as efficient as DeAct-mito in preventing actin accumulation on mitochondria (Fig. 4A-B), possibly as a result of the ER making numerous contacts with mitochondria. Overall, both constructs remained selective for organelle-bound actin as no obvious alterations were found when actin filaments were labeled with phalloidin (Supp. Figure 1C).

Having validated the DeActs, we then evaluated their effect on mitochondrial fusion and fission events. Consistent with the proposed role for ER-associated actin in mitochondrial fission, both DeAct-mito and DeAct-ER significantly decreased mitochondrial fission rates (Fig. 4D). Importantly, mitochondrial fusion was also significantly decreased by both DeActs (Figure 4E), indicating that mitochondria-associated actin is required for mitochondrial fusion. We then determined whether fusion or fission was more affected by DeActs by taking the ratio of fusion over fission for each condition. There was no significant difference in the ratio compared to control cells (mCherry-mito) (~1), suggesting that DeActs blocked both processes (Figure 4F). These data therefore demonstrate an essential role for actin in the regulation of not only mitochondrial fission but also mitochondrial fusion. As previously stated, the majority of fusion events that occurred in the presence of actin were of tip-to-side pattern (Figure 2A-C). We thus then asked whether one type of fusion event was more affected by DeActs. Consistent with tip-to-side events being mostly associated with actin, these were affected to a large extent by DeActs (Fig. 4G). In contrast, tip-to-tip events persisted in DeAct-mito and DeAct-ER transfected cells (Figure 4G), suggesting that the residual fusion observed with DeActs is largely the consequence of actin-independent tip-to-tip fusion events.

Arp2/3-dependent actin polymerization is required for mitochondrial fusion

Having demonstrated that actin is required for mitochondrial fusion, we next defined the role of actin-polymerizing proteins in this process. Most actin polymerization is regulated by one of two families of actin-regulatory proteins: Arp2/3 is responsible for the formation of branched actin filaments and actin patches, while formins promote the formation of parallel actin filaments.

To study the role of Arp2/3 in mitochondrial fusion, we selectively inhibited this nucleation complex using CK-666 (Hetrick et al., 2013). Firstly, there was a notable loss of AC-mito signal following a 60 min CK666 treatment (Fig. 5A-B), supporting a role for Arp2/3 in the generation of mitochondrial actin. The CK-666-dependent loss of mitochondria-associated actin was also associated with a significant decrease in the number of mitochondrial fusion events (Figure 5C). In contrast, CK-666 did not significantly affect mitochondrial fission, resulting in a decrease in the fusion/fission ratio (Figure

5C). As the loss of mitochondrial actin due to the expression of DeAct-mito selectively inhibited tip-to-side fusion (Fig. 4H), we also examined the effect of CK-666 on tip-to-tip and tip-to-side fusion. Consistent with the DeAct data, CK-666 selectively prevented tip-to-side fusion (Fig. 5D). A similar decrease in mitochondrial fusion was also observed in the breast cancer line MDA-MB-231 following CK-666 treatment (Figure 5E). To further confirm our findings, we knocked down Arp2 in MDA-MB-231 cells (Figure 5F) and quantified mitochondrial fission and fusion. Consistent with the CK666 data, mitochondrial fusion was significantly reduced in cells where Arp2 was knocked down. In contrast, mitochondrial fission was not significantly affected, leading to a decrease in fusion/fission ratio (Figure 5G).

To further demonstrate that the Arp2/3 complex is required for mitochondrial fusion, we used a mitochondrial fusion assay based on a mitochondria-targeted photoactivable GFP (PA-GFP). In this assay, diffusion of the activated GFP in a subpopulation of mitochondria following mitochondrial fusion leads to a decrease in GFP fluorescence over time (Figure 5H, Supp. Figure 3). Consistent with Arp2/3 inhibition preventing mitochondrial fusion, PAGFP signal showed a lower rate of decrease in CK666-treated cells compared to control cells, leading to a significantly smaller decrease in GFP signal 3 minutes after activation (Figure 5H).

Altogether, our data shows that inhibition of the Arp2/3 complex significantly impairs mitochondrial fusion, indicating that Arp2/3-dependent actin polymerization plays a crucial role in regulating mitochondrial fusion.

Formin inhibition predominantly affects mitochondrial fission

While our results demonstrate a role for Arp2/3 in mitochondrial fusion, formin proteins are also known to be important for actin dynamics and can both collaborate and compete with Arp2/3 in forming dynamic actin structures (Chan et al., 2019, Cifrova et al., 2020, Dimchev et al., 2021). In addition, both Arp2/3 and formin proteins are known to be important for normal mitochondrial fission dynamics (Moore et al., 2016, Fung et al., 2019, Moore et al., 2021). We thus asked whether formin-mediated actin polymerization could also play a role in mitochondrial fusion. For this, we first used the Formin FH2 Domain Inhibitor (SMIFH2) to inhibit formin-mediated elongation of actin filaments. As with Arp2/3 complex inhibition, formin inhibition resulted in a significant loss of AC-mito signal, but this reduction in mitochondrial actin was less than for Arp2/3 inhibition (Figure 6A-C, Arp inhibition in 5A-B). Consistent with the role of formins in mitochondrial fission, fission was greatly affected by

SMIFH2 (Fig. 6D). On the other hand, while SMIFH2 did reduce mitochondrial fusion, this effect was less important than for fission, leading to a significant increase in the fusion/fission ratio (Fig. 6D). Nevertheless, as for Arp inhibition, SMIFH2 selectively prevented tip-to-side fusion events (Fig. 6E), consistent with actin being predominantly required for this type of fusion event.

The formin protein INF2 is the only known ER-anchored actin regulatory protein and is required for mitochondrial fission (Chakrabarti et al., 2018, Korobova et al., 2013). We thus specifically examined the role of INF2 in fusion by measuring fission and fusion events in U2OS cells lacking INF2 (Chakrabarti et al., 2018). Consistent with our formin inhibitor data, INF2 deletion affected both fission and fusion (Figure 6F). However, contrary to the formin inhibitor, both processes were affected to a similar extent, resulting in a fusion/fission ratio that was similar between control and INF2 KO cells (Figure 6F). Importantly, as with our other manipulations of the actin cytoskeleton, INF2 deletion selectively affected tip-to-side fusion. Altogether, our results indicate that actin is required for tip-to-side events which constitute the majority of fusion events within cells, and that both Arp2/3 and INF2 play a role in this process.

Discussion

Actin plays a critical role in regulating organelle dynamics within cells, contributing to their movement, positioning, and organization (Fung et al., 2023, Lappalainen et al., 2022, Carlsson, 2018). Actin also plays an important role in mitochondrial fission, where it facilitates constriction of mitochondria, the recruitment of DRP1, and the activation of its GTPase activity (Chakrabarti et al., 2018, Hatch et al., 2016, Ji et al., 2015, Liu et al., 2021). Here, we demonstrate that ER- and mitochondria-associated actin is also required for mitochondrial fusion. Specifically, we used organelle-targeted actin chromobodies (Schiavon et al., 2020) to show that mitochondria-associated actin is recruited to mitochondria at sites of both fusion and fission. The ER and ER-associated actin were also present at fusion sites, but they were recruited just before or during fusion at pre-existing actin rich sites on mitochondria. Importantly, we also showed that we can selectively disrupt organelle-associated actin filaments using our novel genetically-encoded DeAct-ER/mito tools. Disrupting mitochondria-associated actin with DeAct-mito expression blocked mitochondrial fusion, demonstrating the importance of mitochondria-associated actin in the regulation of mitochondrial fusion.

Mitochondria-associated actin has previously been reported in a number of settings in addition to mitochondrial fission. For example, actin clouds assemble around depolarised mitochondria to isolate them for autophagy (Fung et al., 2022) while mitochondrial actin comet tails promote mitochondrial redistribution during mitosis (Moore et al., 2021). Distinct actin-polymerizing complexes are likely required depending on the cellular context. For example, two distinct populations of actin filaments have been suggested to regulate fission, the INF2-dependent pathway and a second, INF2-independent but Arp2/3-dependent pathway (Chakrabarti et al., 2018, Fung et al., 2019). These mitochondria-associated actin polymerization processes differ in the cellular stimuli resulting in fission (Korobova et al., 2013, Chakrabarti et al., 2018, Fung et al., 2019). On the other hand, some studies showed that both formins and Arp2/3 are involved in complex-mediated actin assembly around mitochondria (Kruppa et al., 2018, Moore et al., 2016, Chakrabarti et al., 2018). Overall, multiple mechanisms activated on either mitochondria or ER-mitochondria contact sites likely cooperate to stimulate the formation of mitochondria-associated actin filaments. As mitochondria-associated actin has multiple roles, these processes likely play overlapping but distinct roles. Here, as our results show that mitochondria-associated actin marks the site of fusion prior to the recruitment of ER-associated actin

and mitochondrial fusion, we propose that Arp2/3-dependent actin polymerization on mitochondria acts upstream of INF2-dependent polymerization of ER-associated actin during fusion.

We also distinguished two types of mitochondrial fusion events with different requirements for actin. Tip-to-side fusion, which constitute the majority of fusion events and lead to the formation of branched mitochondria, predominantly occurred in the presence of actin. On the other hand, tip-to-tip fusion events, which elongates mitochondria, were much less likely to show actin recruitment. Importantly, disrupting actin polymerization significantly decreased the occurrence of tip-to-side fusion events, but not tip-to-tip events, demonstrating the selectivity of actin for tip-to-side fusion. Interestingly, deletion of ABHD16A, an ER protein regulating the formation of fission and fusion nodes at ER-mitochondria contact sites, results in the loss of tip-to-side fusion (Nguyen and Voeltz, 2022). This suggests that actin could facilitate the formation of these nodes, therefore promoting tip-to-side fusion. These observations may potentially serve as the basis for new insights into genetic and environmental conditions that result in altered branching in mitochondrial networks.

Some studies have noted the presence of elongated mitochondria upon inhibition of actin-polymerizing proteins. While this was seen as evidence for a loss of fission relative to fusion, our results suggest that this could be the result of the lack of requirement for actin during tip-to-tip fusion promoting mitochondrial elongation rather than branching. Another point to take into consideration is the dynamic nature of mitochondrial fission and fusion and the requirement for cells to maintain a balance between the two. For example, INF2 deletion decreased both fusion and fission events. Under these conditions (steady state loss of INF2), it is possible that decrease in fission rates led to a secondary decrease in fusion events to maintain a proper mitochondrial network. On the other hand, we did observe fission events in cells where the Arp2/3 complex was acutely inhibited (one hour treatment). This observation is likely due to the promotion of INF2-dependent fission events. (Chakrabarti et al., 2018, Fung et al., 2019, Korobova et al., 2013, Manor et al., 2015).

Changes in organelle architecture depend on both the inherent composition of membrane lipid bilayers (Hishikawa et al., 2014, Manni et al., 2018) and the external energy necessary to overcome membrane resistance. These external forces include pulling or pushing forces that are generated by cytoskeletal components (Jarsch et al., 2016), including actin. For instance, branched actin assembled at the membrane exerts mechanical forces that alter its curvature (Baldauf et al., 2023). Furthermore, actin-

binding proteins containing a BAR (Bin-Amphiphysin-Rvs) domain can promote membrane curvature through direct membrane interaction and the formation of a scaffold that facilitates membrane curvature and shape cellular structures (Carlsson, 2018, Kessels and Qualmann, 2021). Consistent with this, recent studies have suggested that the actin cytoskeleton is crucial for maintaining the curvature of mitochondrial membranes (Fernandez Casafuz et al., 2023). We speculate that the interaction between the actin cytoskeleton and lipids could thus be crucial for the generation of membrane curvature required for tip-to-side fusion events.

A second potential role of actin in mitochondrial fusion relates to mitochondrial movement. Previous studies have suggested that actin-enriched regions exhibit reduced motility (Korobova et al., 2013, Chakrabarti et al., 2018, Bayraktar et al., 2020). In this context, actin could stabilize or hold the receiving mitochondria in place to enable fusion to occur. Besides, in yeast (Boldogh et al., 2005, Fehrenbacher et al., 2004) and higher plants (Doniwa et al., 2007, Romagnoli et al., 2007), actin filaments can interact with specific motor proteins to regulate short-distance mitochondrial movement, which could also serve to properly align the two fusing mitochondria. As the role of actin filaments in mitochondrial movement is likely context-dependent, both processes could control the position and stability of the receiving mitochondrion which might be crucial for efficient mitochondrial fusion. In this context, it is interesting to note that both mitochondria and ER-associated actin are recruited to fusion sites, as these two pools of actin may act at different steps in the fusion process.

A third potential role for actin in mitochondrial fusion relates to actin's well-established role in promoting the GTPase activity of dynamin-related proteins. While this is relatively well-established for DRP1 in mitochondrial fission, more work must be done to clarify whether actin also facilitates MFN1/2 GTPase activity. However, our data showing increased mitochondria-associated actin in cells overexpressing MFN1 certainly suggests some form of crosstalk between MFN1-mediated fusion and mitochondria-associated actin. Future studies will be needed to clarify these results and further elucidate the mechanisms by which actin facilitates mitochondrial fusion.

In summary, our findings emphasize the significant role of actin polymerization in organizing tip-to-side fusion events. However, unlike during fission, where actin is known to form constrictions, the functional aspect of actin during fusion remains yet to be elucidated. Further research is needed to gain a better understanding of the role of actin in fusion and its localization. Our study highlights the

multifunctionality of actin in regulating organelle dynamics, emphasizing the need for continued investigation in this area.

Material and Methods

Cell culture:

Control Primary Human Fibroblasts were purchased from the Coriell institute and cultured in Dulbecco's modified Eagle's medium (DMEM) containing 10% fetal bovine serum (FBS), supplemented with Penicillin/Streptomycin (100 IU/ml/100µL/mL). MDA-MB-231 cells (triple negative breast cancer) were purchased from ATCC and cultured in DMEM supplemented with 10% fetal bovine serum. These cells were stably transfected with mitochondria-targeted GFP (CCOeGFP, addgene, pLVX-EF1a-CCO-IRES, #134861) using Metafectene (Biontex). Cell culture reagents were obtained from Wisent.

Plasmids and Transient transfection of primary cells

Primary cells were trypsinized and centrifuged at 5000rpm for 5 minutes. Cell pellets were suspended in 10µl of the Neon transfection buffer R (ThermoFisher Scientific, MPK1096). Cells were transiently transfected with EF1a-CCO-IRES (addgene #134861), mito-PAGFP (addgene, #23348), Mfn1-Myc (addgene #23212), mCherry-Fis1, mCherry-Cytb5, Halo-Fis1 and all custom actin nanobody probes that we previously reported (Schiavon et al., 2020) using the Neon transfection system (ThermoFisher Scientific, MPK5000) according to the manufacturer's protocol. For all experiments, 1 µg of total DNA concentrations were transfected per 10ul of 10^6cells/ml (individually or combined for co-transfection). DeAct-ER and DeAct-Mito constructs where generated utilizing the "Gelsolin Segment 1 (GS1)" sequence described in Harterink et al (Harterink et al.). The GS1 sequence was cloned into the pSIN vector under a CMV promoter, N-terminal to the mScarlet fluorescent protein sequence. Either a Cytb5ER or Fis1 localization sequence was fused to the mScarlet C-terminus to target expression to the ER (DeAct-ER) or mitochondrial outer membrane (DeAct-Mito), respectively. Cytb5ER and Fis1 targeting sequences are the same as those previously described in Schiavon et al. (Schiavon et al., 2020) to target AC-ER and AC-Mito to the ER or mitochondrial outer membrane.

siRNA treatment

MDA-MB-231 were seeded onto 6 well dishes to reach 30–40% density in 24 hours. Then the cells were transfected with 10 nM of Arp2 siRNA (Dharmacon reagents, ACTR2 Gene 10097) and control siRNA (Thermo Fisher Scientific, Silencer Select, 4390843) using siLenFect lipid reagent (Bio-Rad,1703361). After 24 hours, the cells were imaged live or collected for western blotting.

Drug treatments.

Cells were incubated with 10 μM CK-666 (CAS 442633-00-3 – Calbiochem) or Formin FH2 Domain Inhibitor, SMIFH2 (CAS 340316-62-3 – Calbiochem) for 60 minutes to inhibit Arp2/3 complex and formins, respectively.

Immunofluorescence:

Transfected cells were seeded onto glass coverslips (Fisherbrand, 1254580) and allowed to adhere overnight. Cells were fixed with 4% paraformaldehyde for 15 minutes at room temperature (RT). Cells were then permeabilized with 0.2% Triton X-100 in PBS and blocked with 1% BSA / 0.1% Triton X-100 in PBS. The cells were then incubated with primary antibodies using following antibodies as per the experiment: TOM20 (Rb, Abcam, ab186735, 1:250), RTN4/NOGOA (Rb, Bio-Rad, AHP1799, 1:200), followed by with fluorescent tagged secondary antibodies (Jackson Immunoresearch, 1:500) and DAPI (Invitrogen, Thermo Fisher, D1306, 1:100).

Live imaging and confocal microscopy

For Live cell microscopy imaging, cells were grown on glass bottom dishes in complete medium and stained for 30 min with 250 nM TMRM (Thermo fisher Scientific, T668) or 5 min with 100nM Mitotracker Deep Red (Thermo fisher scientific, M7512) where indicated. After staining, cells were washed 3 times with pre-warmed 1× phosphate buffered saline (PBS), and normal growth media was added prior to imaging. The plates were mounted onto Leica TSC SP8 confocal microscope fitted with a 63×/1.40 oil objective using the optimal resolution for the wavelength (determined using the Leica software). Time-lapse images were acquired at a speed of (0.05-0.125 frames/s) for 10 minutes.

For the INF2 experiments, Wild-type and INF2 KO U2OS cells (Chakrabarti et al., 2018) were maintained in DMEM supplemented with 10% FBS at 37C with 5% CO2. Cells were plated on 8-well no. 1.5 imaging chambers (Cellvis) coated with 10ug/mL fibronectin. Cells were stained with 50nM MitoTracker Deep Red for 30min, washed with PBS, then imaged in FluoroBright medium (Thermo Fisher) supplemented with 10% FBS. Cells were imaged with a C-Apochromat x40/1.2 NA W Korr FCS M27 objective on an inverted Zeiss 880 LSM Airyscan confocal microscope with the environmental control system supplying 37C, 5% CO2, and humidity for live-cell imaging. MitoTracker Deep Red was imaged with a 647-nm laser line at ~250nW laser power at optimal resolution (determined by Zen Black software). Time-lapses were acquired at a speed of 0.152-0.357

frames/s for 5min. Following acquisition, images were Airyscan processed using auto-filter 2D-SR settings in Zen Blue.

Image processing and analysis:

All image manipulation and analysis were done in Image J/Fiji. The images shown are from single focal planes unless stated otherwise. For mitochondrial area, the images were segmented in ImageJ using Filter/Median (1.0), then thresholding and adjusting the resulting image using Binary/Erode. Total mitochondria area was then measured using the measure function.

Tracking of Fusion and Fission events

Quantification of fusion and fission events was done manually. The images were tracked frame by frame to record movement of mitochondria that resulted in fusion or fission. Stable separation of the mitochondrial marker was counted as a fission event. Fusion events were defined as follows: two fusing mitochondria must retain their fused state for the following 5 frames (i.e 60sec). If there was a division at the fusion site within 5 frames, such an event is discarded. Also, the mean signal intensity of the mitochondrial marker at the site of fusion and a region elsewhere on mitochondria (basal) was recorded at the end of the 5 frames. If the ratio of signal intensity at the site of fusion and basal signal intensity was higher than 1, it was considered as an overlapping, not a fusion event. The presence of ER at the site of fusion or fission was also assessed manually, by looking for ER colocalizing with mitochondria at the site.

Tracking of AC-mito and AC-ER at fusion sites

To identify when actin is accumulated on ER and mitochondria relative to a fusion event, we counted backwards from that fusion event to determine at which frame the AC probe accumulated on mitochondria and ER. Determining the time between the frames where AC-mito and AC-ER appear at the fusion site gives us the information on the time taken by Actin to get accumulated on the organelle.

AC probe 'accumulation' calculation.

Using Fiji, a square selection was drawn around a region with obvious AC probe accumulation (0.8 μm^2 for mitochondria and ER). The mean pixel intensity of AC-GFP and mCherry channels was measured within the selection. Another square of equal dimensions was drawn in an adjacent, control

area with mCherry signal and mean pixel intensity was measured. The mean pixel intensity in the accumulated region was then divided by the mean pixel intensity in the control region.

Mean AC Signal Intensity

The loss or gain of AC probe signal was determined in cells transfected with DeActs, Mfn1 or upon treatment with inhibitors for Arp2/3 complex and formins. The integrated density of AC-Mito/ AC-ER signal of individual cells was measured in Fiji. For AC-mito mean signal intensity, the integrated density signal was then divided by mitochondrial area. For AC-ER, the integrated density was divided by the cell area. The loss or gain of the AC probe signal was obtained by comparing the values to that of the control. The imaging parameters (laser intensity and gain values) were kept identical for control and test conditions for every experiment.

mtPA-GFP-based Mitochondrial Fusion Assay

The photoactivation-based fusion assay (Karbowski et al., 2014) was conducted by expressing Mito-PAGFP (Addgene #23348) in primary human fibroblasts. The cells were co-stained with TMRM to monitor mitochondrial membrane potential. Photoactivation was performed in selected ROIs using the 405 nm laser with 100% power and 40 iterations. Upon activation of mito-PAGFP, a small portion of the mitochondrial network is photoactivated, and the spread or loss of the signal to the rest of the mitochondrial network was recorded in the ROIs. The signal of all ROIs with significant PAGFP activation within a cell was then averaged and normalized to the initial signal intensity post-activation.

Western Blot

Cells were lysed in 10 mM Tris-HCl, pH 7.4, 1mM EDTA, 150 mM NaCl, 1% Triton X-100, complemented with a protease inhibitor cocktail (Sigma-Aldrich) and phosphatase inhibitor (Sigma-Aldrich), kept on ice for 10 min and centrifuged at 13000rpm for 10 minutes. Protein supernatants were collected, and protein concentration was estimated by DC protein assay kit (BioRad). For SDS-PAGE, 30 µg of proteins were mixed with 1X Lammeli buffer containing β-mercaptoethanol, then subjected to SDS-PAGE, transferred to a nitrocellulose membrane and blotted with the indicated antibodies (Arp2 (Santacruz, (E-12): sc-166103, 1:1000), HRP-tagged Actin (1:10,000). Membranes were then incubated with a 1:5000 dilution of horseradish peroxidase-conjugated secondary antibodies (Jackson Immunoresearch) and visualized by enhanced chemiluminescence (Thermo Fisher scientific) using a Bio-Rad imaging system.

Data analysis and statistics

All graphs and statistical analysis were done using R. Immunofluorescence data were quantified and images representative of at least three independent experiments shown (exact n are in the quantification figures). Data is represented as average ± SD as specified in figure legends. Statistical significance was determined using Student's t test (between 2 groups) or one-way ANOVA with a tukey post hoc test (multiple comparisons). Individual experiments are noted as different colour shades in the graphs.

Acknowledgements

HSI was supported by a Queen Elizabeth II Diamond Jubilee Scholarship and a FRQS scholarship. This work was supported by grants from the Natural Sciences and Engineering Research Council of Canada to MG. U.M. is a Chan-Zuckerberg Initiative Imaging Scientist and supported by NSF NeuroNex Award 2014862, NIH-NIA Nathan Shock Center P30 AG068635-01, and the LIFE Foundation. NIH 1F32GM137580 to C.R.S. This work was also supported by the Waitt Advanced Biophotonics Core Facility of the Salk Institute with funding from NIH-NCI CCSG: P30 014195, and the Waitt Foundation.

References

ABRISCH, R. G., GUMBIN, S. C., WISNIEWSKI, B. T., LACKNER, L. L. & VOELTZ, G. K. 2020. Fission and fusion machineries converge at ER contact sites to regulate mitochondrial morphology. *J Cell Biol,* 219.

BALDAUF, L., FREY, F., ARRIBAS PEREZ, M., IDEMA, T. & KOENDERINK, G. H. 2023. Branched actin cortices reconstituted in vesicles sense membrane curvature. *Biophys J*.

BAYRAKTAR, S., NEHRIG, J., MENIS, E., KARLI, K., JANNING, A., STRUK, T., HALBRITTER, J., MICHGEHL, U., KRAHN, M. P., SCHUBERTH, C. E., PAVENSTADT, H. & WEDLICH-SOLDNER, R. 2020. A Deregulated Stress Response Underlies Distinct INF2-Associated Disease Profiles. *J Am Soc Nephrol,* 31**,** 1296-1313.

BOLDOGH, I. R., FEHRENBACHER, K. L., YANG, H. C. & PON, L. A. 2005. Mitochondrial movement and inheritance in budding yeast. *Gene,* 354**,** 28-36.

CARLSSON, A. E. 2018. Membrane bending by actin polymerization. *Curr Opin Cell Biol,* 50**,** 1-7.

CHAKRABARTI, R., JI, W. K., STAN, R. V., DE JUAN SANZ, J., RYAN, T. A. & HIGGS, H. N. 2018. INF2-mediated actin polymerization at the ER stimulates mitochondrial calcium uptake, inner membrane constriction, and division. *J Cell Biol,* 217**,** 251-268.

CHAN, F. Y., SILVA, A. M., SARAMAGO, J., PEREIRA-SOUSA, J., BRIGHTON, H. E., PEREIRA, M., OEGEMA, K., GASSMANN, R. & CARVALHO, A. X. 2019. The ARP2/3 complex prevents excessive formin activity during cytokinesis. *Mol Biol Cell,* 30**,** 96-107.

CHANDEL, N. S. 2015. Evolution of Mitochondria as Signaling Organelles. *Cell Metab,* 22**,** 204-6.

CHEN, H., DETMER, S. A., EWALD, A. J., GRIFFIN, E. E., FRASER, S. E. & CHAN, D. C. 2003. Mitofusins Mfn1 and Mfn2 coordinately regulate mitochondrial fusion and are essential for embryonic development. *J Cell Biol,* 160**,** 189-200.

CIFROVA, P., OULEHLOVA, D., KOLLAROVA, E., MARTINEK, J., ROSERO, A., ZARSKY, V., SCHWARZEROVA, K. & CVRCKOVA, F. 2020. Division of Labor Between Two Actin Nucleators-the Formin FH1 and the ARP2/3 Complex-in Arabidopsis Epidermal Cell Morphogenesis. *Front Plant Sci,* 11**,** 148.

DETMER, S. A. & CHAN, D. C. 2007. Functions and dysfunctions of mitochondrial dynamics. *Nat Rev Mol Cell Biol,* 8**,** 870-9.

DIMCHEV, V., LAHMANN, I., KOESTLER, S. A., KAGE, F., DIMCHEV, G., STEFFEN, A., STRADAL, T. E. B., VAUTI, F., ARNOLD, H. H. & ROTTNER, K. 2021. Induced Arp2/3 Complex Depletion Increases FMNL2/3 Formin Expression and Filopodia Formation. *Front Cell Dev Biol,* 9**,** 634708.

DONIWA, Y., ARIMURA, S.-I. & TSUTSUMI, N. 2007. Mitochondria use actin filaments as rails for fast translocation in Arabidopsis and tobacco cells. *Plant Biotechnology,* 24**,** 441-447.

FEHRENBACHER, K. L., YANG, H. C., GAY, A. C., HUCKABA, T. M. & PON, L. A. 2004. Live cell imaging of mitochondrial movement along actin cables in budding yeast. *Curr Biol,* 14**,** 1996-2004.

FERNANDEZ CASAFUZ, A. B., DE ROSSI, M. C. & BRUNO, L. 2023. Mitochondrial cellular organization and shape fluctuations are differentially modulated by cytoskeletal networks. *Sci Rep,* 13**,** 4065.

FRIEDMAN, J. R., LACKNER, L. L., WEST, M., DIBENEDETTO, J. R., NUNNARI, J. & VOELTZ, G. K. 2011. ER tubules mark sites of mitochondrial division. *Science,* 334**,** 358-62.

FUNG, T. S., CHAKRABARTI, R. & HIGGS, H. N. 2023. The multiple links between actin and mitochondria. *Nat Rev Mol Cell Biol*.

FUNG, T. S., CHAKRABARTI, R., KOLLASSER, J., ROTTNER, K., STRADAL, T. E. B., KAGE, F. & HIGGS, H. N. 2022. Parallel kinase pathways stimulate actin polymerization at depolarized mitochondria. *Curr Biol,* 32**,** 1577-1592 e8.

FUNG, T. S., JI, W. K., HIGGS, H. N. & CHAKRABARTI, R. 2019. Two distinct actin filament populations have effects on mitochondria, with differences in stimuli and assembly factors. *J Cell Sci,* 132.

GU, C., CHANG, J., SHCHEDRINA, V. A., PHAM, V. A., HARTWIG, J. H., SUPHAMUNGMEE, W., LEHMAN, W., HYMAN, B. T., BACSKAI, B. J. & SEVER, S. 2014. Regulation of dynamin oligomerization in cells: the role of dynamin-actin interactions and its GTPase activity. *Traffic,* 15**,** 819-38.

GU, C., YADDANAPUDI, S., WEINS, A., OSBORN, T., REISER, J., POLLAK, M., HARTWIG, J. & SEVER, S. 2010. Direct dynamin-actin interactions regulate the actin cytoskeleton. *EMBO J,* 29**,** 3593-606.

GUO, Y., LI, D., ZHANG, S., YANG, Y., LIU, J. J., WANG, X., LIU, C., MILKIE, D. E., MOORE, R. P., TULU, U. S., KIEHART, D. P., HU, J., LIPPINCOTT-SCHWARTZ, J., BETZIG, E. & LI, D. 2018. Visualizing Intracellular Organelle and Cytoskeletal Interactions at Nanoscale Resolution on Millisecond Timescales. *Cell,* 175**,** 1430-1442 e17.

HATCH, A. L., GUREL, P. S. & HIGGS, H. N. 2014. Novel roles for actin in mitochondrial fission. *J Cell Sci,* 127**,** 4549-60.

HATCH, A. L., JI, W. K., MERRILL, R. A., STRACK, S. & HIGGS, H. N. 2016. Actin filaments as dynamic reservoirs for Drp1 recruitment. *Mol Biol Cell,* 27**,** 3109-3121.

HETRICK, B., HAN, M. S., HELGESON, L. A. & NOLEN, B. J. 2013. Small molecules CK-666 and CK-869 inhibit actin-related protein 2/3 complex by blocking an activating conformational change. *Chem Biol,* 20**,** 701-12.

HISHIKAWA, D., HASHIDATE, T., SHIMIZU, T. & SHINDOU, H. 2014. Diversity and function of membrane glycerophospholipids generated by the remodeling pathway in mammalian cells. *J Lipid Res,* 55**,** 799-807.

HUANG, P., YU, T. & YOON, Y. 2007. Mitochondrial clustering induced by overexpression of the mitochondrial fusion protein Mfn2 causes mitochondrial dysfunction and cell death. *Eur J Cell Biol,* 86**,** 289-302.

JARSCH, I. K., DASTE, F. & GALLOP, J. L. 2016. Membrane curvature in cell biology: An integration of molecular mechanisms. *J Cell Biol,* 214**,** 375-87.

JI, W. K., HATCH, A. L., MERRILL, R. A., STRACK, S. & HIGGS, H. N. 2015. Actin filaments target the oligomeric maturation of the dynamin GTPase Drp1 to mitochondrial fission sites. *Elife,* 4**,** e11553.

KARBOWSKI, M., CLELAND, M. M. & ROELOFS, B. A. 2014. Photoactivatable green fluorescent protein-based visualization and quantification of mitochondrial fusion and mitochondrial network complexity in living cells. *Methods Enzymol,* 547**,** 57-73.

KESSELS, M. M. & QUALMANN, B. 2021. Interplay between membrane curvature and the actin cytoskeleton. *Curr Opin Cell Biol,* 68**,** 10-19.

KOROBOVA, F., GAUVIN, T. J. & HIGGS, H. N. 2014. A role for myosin II in mammalian mitochondrial fission. *Curr Biol,* 24**,** 409-14.

KOROBOVA, F., RAMABHADRAN, V. & HIGGS, H. N. 2013. An actin-dependent step in mitochondrial fission mediated by the ER-associated formin INF2. *Science,* 339**,** 464-7.

KRUPPA, A. J., KISHI-ITAKURA, C., MASTERS, T. A., RORBACH, J. E., GRICE, G. L., KENDRICK-JONES, J., NATHAN, J. A., MINCZUK, M. & BUSS, F. 2018. Myosin VI-Dependent Actin Cages Encapsulate Parkin-Positive Damaged Mitochondria. *Dev Cell,* 44**,** 484-499 e6.

LAPPALAINEN, P., KOTILA, T., JEGOU, A. & ROMET-LEMONNE, G. 2022. Biochemical and mechanical regulation of actin dynamics. *Nat Rev Mol Cell Biol,* 23**,** 836-852.

LEGROS, F., LOMBES, A., FRACHON, P. & ROJO, M. 2002. Mitochondrial fusion in human cells is efficient, requires the inner membrane potential, and is mediated by mitofusins. *Mol Biol Cell,* 13**,** 4343-54.

LI, S., XU, S., ROELOFS, B. A., BOYMAN, L., LEDERER, W. J., SESAKI, H. & KARBOWSKI, M. 2015. Transient assembly of F-actin on the outer mitochondrial membrane contributes to mitochondrial fission. *J Cell Biol,* 208**,** 109-23.

LIU, A., KAGE, F. & HIGGS, H. N. 2021. Mff oligomerization is required for Drp1 activation and synergy with actin filaments during mitochondrial division. *Mol Biol Cell,* 32**,** ar5.

LOPEZ-DOMENECH, G., COVILL-COOKE, C., IVANKOVIC, D., HALFF, E. F., SHEEHAN, D. F., NORKETT, R., BIRSA, N. & KITTLER, J. T. 2018. Miro proteins coordinate microtubule- and actin-dependent mitochondrial transport and distribution. *EMBO J,* 37**,** 321-336.

MANNI, M. M., TIBERTI, M. L., PAGNOTTA, S., BARELLI, H., GAUTIER, R. & ANTONNY, B. 2018. Acyl chain asymmetry and polyunsaturation of brain phospholipids facilitate membrane vesiculation without leakage. *Elife,* 7.

MANOR, U., BARTHOLOMEW, S., GOLANI, G., CHRISTENSON, E., KOZLOV, M., HIGGS, H., SPUDICH, J. & LIPPINCOTT-SCHWARTZ, J. 2015. A mitochondria-anchored isoform of the actin-nucleating spire protein regulates mitochondrial division. *Elife,* 4.

MOORE, A. S., COSCIA, S. M., SIMPSON, C. L., ORTEGA, F. E., WAIT, E. C., HEDDLESTON, J. M., NIRSCHL, J. J., OBARA, C. J., GUEDES-DIAS, P., BOECKER, C. A., CHEW, T. L., THERIOT, J. A., LIPPINCOTT-SCHWARTZ, J. & HOLZBAUR, E. L. F. 2021. Actin cables and comet tails organize mitochondrial networks in mitosis. *Nature,* 591**,** 659-664.

MOORE, A. S., WONG, Y. C., SIMPSON, C. L. & HOLZBAUR, E. L. 2016. Dynamic actin cycling through mitochondrial subpopulations locally regulates the fission-fusion balance within mitochondrial networks. *Nat Commun,* 7**,** 12886.

NGUYEN, T. T. & VOELTZ, G. K. 2022. An ER phospholipid hydrolase drives ER-associated mitochondrial constriction for fission and fusion. *Elife,* 11.

ROMAGNOLI, S., CAI, G., FALERI, C., YOKOTA, E., SHIMMEN, T. & CRESTI, M. 2007. Microtubule- and actin filament-dependent motors are distributed on pollen tube mitochondria and contribute differently to their movement. *Plant Cell Physiol,* 48**,** 345-61.

SCHIAVON, C. R., ZHANG, T., ZHAO, B., MOORE, A. S., WALES, P., ANDRADE, L. R., WU, M., SUNG, T. C., DAYN, Y., FENG, J. W., QUINTERO, O. A., SHADEL, G. S., GROSSE, R. & MANOR, U. 2020. Actin chromobody imaging reveals sub-organellar actin dynamics. *Nat Methods,* 17**,** 917-921.

SHIRIHAI, O. S., SONG, M. & DORN, G. W., 2ND 2015. How mitochondrial dynamism orchestrates mitophagy. *Circ Res,* 116**,** 1835-49.

TAN, J. X. & FINKEL, T. 2020. Mitochondria as intracellular signaling platforms in health and disease. *J Cell Biol,* 219.

YANG, C. & SVITKINA, T. M. 2019. Ultrastructure and dynamics of the actin-myosin II cytoskeleton during mitochondrial fission. *Nat Cell Biol,* 21**,** 603-613.

Figure legends

Figure 1. Actin marks the site of mitochondrial fusion. (A) Representative fusion event showing the enrichment of AC-mito at the fusion site (arrowhead). Cells were transfected with mCherry-mito (mitochondria, magenta) and AC-mito (actin, green). Scale bar 2µm (B) Quantification of fission (Fis.) and fusion (Fus.) events positive for AC-mito. Each point represents an individual cell, with 10 cells quantified in 4 independent experiments. Bars show the average ± SD. (C-D) AC-mito signal enrichment at fusion (C) and fission (D) sites in cells transfected as in A. Signal intensity at the event site relative to an adjacent site on the mitochondrial network was quantified for AC-mito (AC) and mCherry-mito (mCh). Each point represents an individual cell, with 8 cells quantified in 4 independent experiments. Bars show the average ± SD. *** $p<0.001$. (E-F) Representative image showing AC-mito signal (green) in cells transfected with mCherry-Fis1 (Control) or MFN1-Myc. Cells were then fixed, and mitochondria labeled with an antibody against TOM20 (magenta). Quantification of the AC-mito signal is shown in (F). Each point represents an individual cell, with 28 control and 32 MFN1-Myc cells quantified in 3 independent experiments. Bars show the average ± SD. *** $p<0.001$. Scale bar 10 µm.

Figure 2. Actin is mainly associated with Tip-to-side mitochondrial fusion (A) Schematic representation of Tip-to-tip and Side-to-End fusion events. (B-C) Quantification of fusion events as end to-side (Side) or tip-to-tip (End)(B), and their corresponding association with AC-mito (C). Each point represents an individual cell, with 10 cells (E) quantified in 4 independent experiments. Bars show the average ± SD. *** $p<0.001$. Total events from the quantified cells are shown in (C). (D-E) Quantification of fusion events containing one immobile mitochondrion (Still) or two mobile mitochondria (Mobile) (D) and their corresponding association with AC-mito (E). Each point represents an individual cell 8 cells quantified in 4 independent experiments. Bars show the average ± SD. *** $p<0.001$. Total events from the quantified cells are shown in (E). (F) Quantification of AC-mito signal associated with each of the fusing mitochondria (the receiving mitochondrion (Rec) and the fusing mitochondrion (Fus)) as well as with the fusion site one frame post-fusion (Post). Each point represents an individual cell, with 9 cells quantified in 4 independent experiments. Bars show the average ± SD. * $p<0.05$, ** $p<0.01$

Figure 3. ER-associated actin is present at the site of mitochondrial fusion. (A) Quantification of fission (Fis.) and fusion (Fus.) events associated with ER. Each point represents an individual cell, with 15 cells quantified in 4 independent experiments. Bars show the average ± SD. (B) Representative fusion event showing the enrichment of AC-ER at the fusion site (arrowhead). Cells were transfected with mCherry-mito (mitochondria, magenta) and AC-ER (actin, green). Scale bar 2 μm. (C) Quantification of fission (Fis.) and fusion (Fus.) events positive for AC-mito. Each point represents an individual cell, with 13 cells quantified in 3 independent experiments. (D-E) AC-ER signal enrichment at fusion (D) and fission (E) sites in cells transfected as in B. Signal intensity at the event site relative to an adjacent site on the ER network was quantified for AC-ER (AC) and mCherry-ER (mCh). Each point represents an individual cell, with 13 cells quantified in 3 independent experiments. Bars show the average ± SD. *** $p<0.001$. (F) Quantification of AC-ER signal associated with each of the fusing mitochondria (the receiving mitochondrion (Rec) and the fusing mitochondrion (Fus)) as well as with the fusion site one frame post-fusion (Post). Each point represents an individual cell, with 13 cells quantified in 3 independent experiments. Bars show the average ± SD. * $p<0.05$, ** $p<0.01$. (G-H) Kinetics of recruitment of AC-mito and AC-ER at the fusion site showing AC-ER recruitment relative to AC-mito (G) and recruitment of either marker relative to the time of fusion (H). Each point represents an individual event (20 events total in 4 cells within 3 independent experiments). *** $p<0.001$

Figure 4. Mitochondrial actin is required for both fission and fusion. (A) Representative images showing the loss of AC-mito signal (green) in cells transfected with DeAct-mito or DeAct-ER (magenta). (B-C) Quantification of AC-mito (B) and AC-ER (C) signal in cells transfected as in (A). Each point represents an individual cell, with at least 8 cells quantified in 3 independent experiments for each condition. Bars show the average ± SD. *** $p<0.001$, ** $p<0.01$. (D-F) Quantification of the number of fission (D) and fusion (E) events, as well as the fusion/fission ratio (F) in cells transfected with the indicated DeAct probe, AC-mito and mCherry-Fis1 (to label mitochondria). Each point represents an individual cell, with 11 (mCh), 8 (DeAct-mito) and 9 (DeAct-ER) cells quantified in 3 independent experiments. Bars show the average ± SD. ** $p<0.01$, * $p<0.05$.

(G) Quantification of fusion events as end to-side (Side) or tip-to-tip (End). The total number of events for 8 cells in 3 experiments is shown for each condition.

Figure 5. The Arp2/3 complex regulates mitochondrial fusion. (A) Representative images showing the loss of AC-mito signal in primary fibroblasts transfected with AC-mito (green) and mCherry-Fis1 (magenta), and treated with the Arp2 inhibitor CK666. Scale bar 10 μm (B) Quantification of AC-mito signal in cells transfected as in (A). Each point represents an individual cell, with 12 control and 13 CK666 cells quantified in 3 independent experiments. Bars show the average ± SD. *** $p<0.001$. (C) Quantification of the number of fusion (Left, blue) and fission (Middle, orange) events, as well as the fusion/fission ratio (Right) in cells transfected as in (A) and treated as indicated. Each point represents an individual cell, with 12 (control) and 9 (CK666) cells quantified in 3 independent experiments. Bars show the average ± SD. ** $p<0.01$, * $p<0.05$. (D) Quantification of fusion events as end to-side (Side) or tip-to-tip (End). The total number of events for 9 cells in 3 experiments is shown for each condition. (E) Quantification of the number of fusion (Left, blue) and fission (Middle, orange) events, as well as the fusion/fission ratio (Right) in MDA-MB-231 cells stably expressing mitochondria-targeted GFP and treated as indicated. Each point represents an individual cell, with 10 cells quantified for each condition in 3 independent experiments. Bars show the average ± SD. *** $p<0.001$, * $p<0.05$. (F) Western blot showing Arp2 expression in cells treated with a control siRNA (siCtrl) or a siRNA against ARP2 (siARP2). Actin is used as a loading control. (G) Quantification of the number of fusion (Left, blue) and fission (Middle, orange) events, as well as the fusion/fission ratio (Right) in MDA-MB-231 cells stably expressing mitochondria-targeted GFP transfected with siRNAs as in (F). Each point represents an individual cell, with 10 cells quantified for each condition in 3 independent experiments. Bars show the average ± SD. *** $p<0.001$, ** $p<0.01$. (H) Mitochondrial fusion assay. Human primary fibroblasts were transfected with photoactivatable-GFP (PA-GFP), treated as indicated and imaged before (pre) and after activation with the 405 nm laser. Fluorescence traces (Left) and the quantification of the loss of fluorescence at 3 min relative to the initial time post-activation (Right) are shown. Each point (Right) represents an individual cell, with 14 ctrl and 16 CK666 cells quantified in 4 independent experiments. Bars show the average ± SD. ** $p<0.01$

Figure 6. Formin-dependent regulation of mitochondrial fusion. (A) Representative images showing AC-mito signal in primary fibroblasts transfected with AC-mito (green) and mCherry-Fis1 (magenta), and treated with the formin inhibitor SMIFH2. Scale bar 10 μm (B) Quantification of AC-mito signal in cells transfected as in (A). Each point represents an individual cell, with 12 cells quantified in 3 independent experiments. Bars show the average ± SD. *** $p<0.001$. (C) Loss of AC-mito signal caused by CK666 and SMIFH2 relative to control levels. CK666 data from Figure 5B, SMIFH2 data from panel (B) above. Individual points represent independent experiments. Bars show the average ± SD. ** $p<0.01$. (D) Quantification of the number of fusion (Left, blue) and fission (Middle, orange) events, as well as the fusion/fission ratio (Right) in cells transfected as in (A) and treated as indicated. Each point represents an individual cell, with 12 cells quantified in 3 independent experiments. Bars show the average ± SD. *** $p<0.001$, ** $p<0.01$. (E) Quantification of fusion events as end to-side (Side) or tip-to-tip (End). The total number of events for 12 cells in 3 experiments is shown for each condition. (F-G) Quantification of the number of fusion (Left, blue) and fission (Middle, orange) events, as well as the fusion/fission ratio (Right) in U2OS cells in which INF2 has been deleted using CRISPR/Cas9. Each point represents an individual cell, with 12 cells quantified in 3 independent experiments. Bars show the average ± SD. ** $p<0.01$. (G) Quantification of fusion events as end to-side (Side) or tip-to-tip (End). The total number of events for 12 cells in 3 experiments is shown for each condition.

Supplemental Figure 1. Proper targeting of DeActs. (A) Representative images of primary human fibroblasts transfected with DeAct-mito (magenta) and marked with an antibody against TOM20 (mitochondria, green). The boxed area is shown enlarged below the main image. (B) Representative images of cells transfected with DeAct-ER (magenta) and marked with an antibody against RTN4 (ER, green). The boxed area is shown enlarged below the main image. (C) DeActs do not affect overall actin filaments. Cells were transfected as in (A-B) and stained with phalloidin (actin, green). Scale bar 10 μm, 2 μm for the enlarged images.

Supplemental Figure 2. DeAct-ER inhibits the polymerization of ER-associated actin. Representative images showing the loss of AC-ER signal (green) in cells transfected with DeAct--ER (magenta).

Supplemental Figure 3. Representative images of the fusion assay. Representative images of human primary fibroblasts transfected with photoactivatable-GFP (PA-GFP) were treated as indicated and imaged immediately after activation (Post-activation) and 100 sec following a fusion event. Scale bar 2 μm.

Figure 1

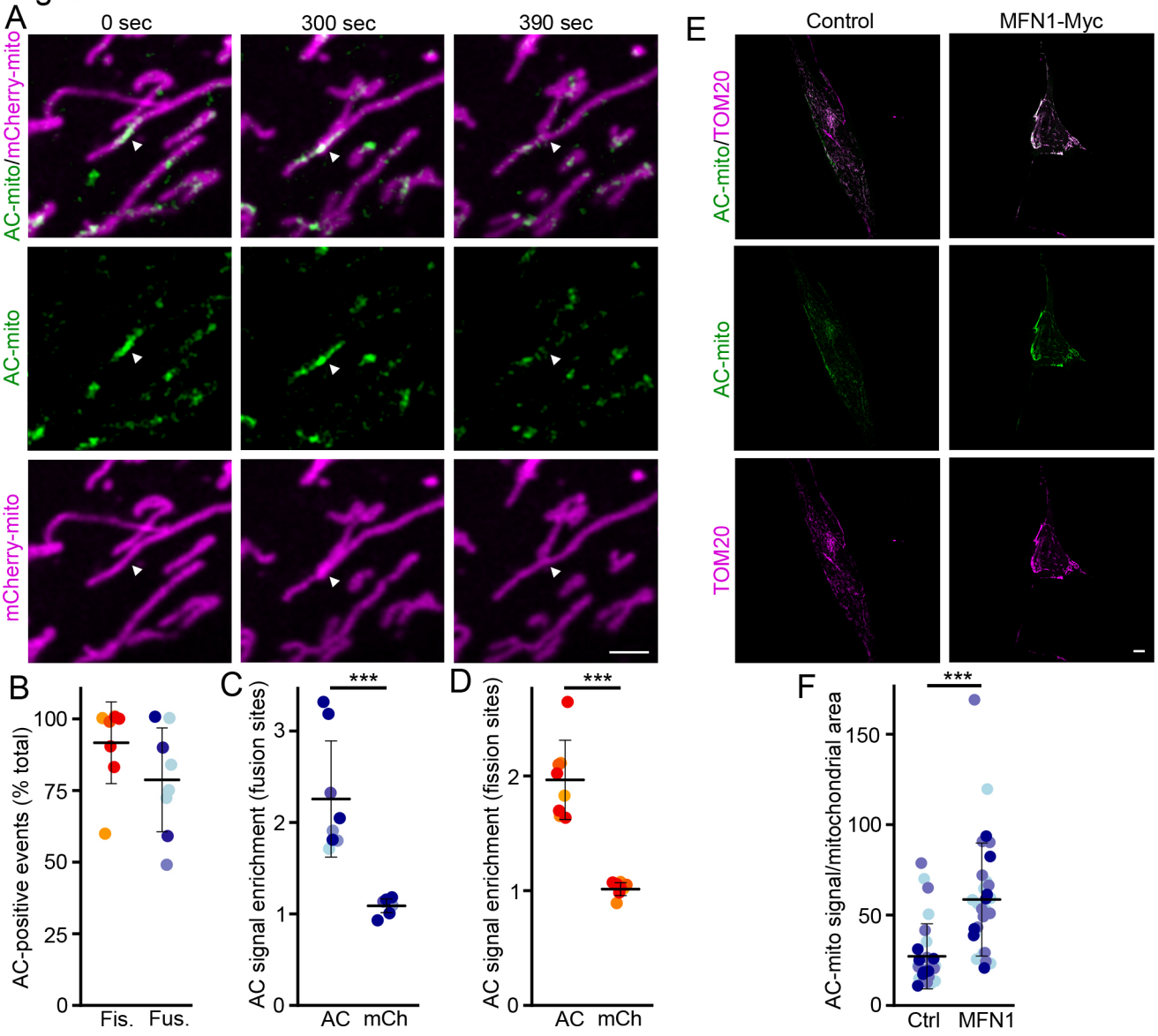

Figure 2

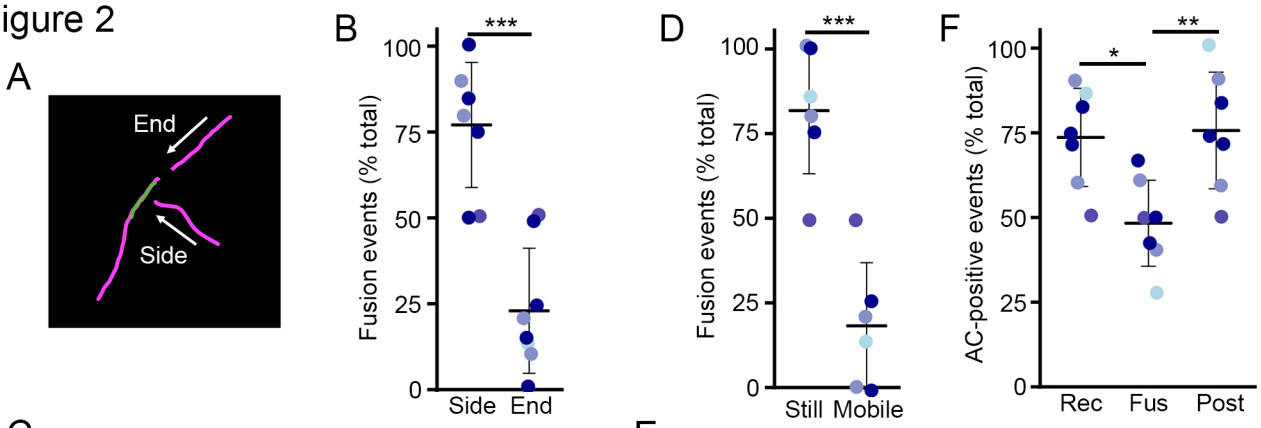

C

AC accumulation relative to type of fusion

Type	AC-positive	Percent AC
End-to-End	4/8	50%
End-to-Side	30/34	88%

E

Presence of one mobile end relative to type of fusion

Type	Mobile	Percent Mobile
End-to-End	4/5	80%
End-to-Side	0/26	0%

Figure 3

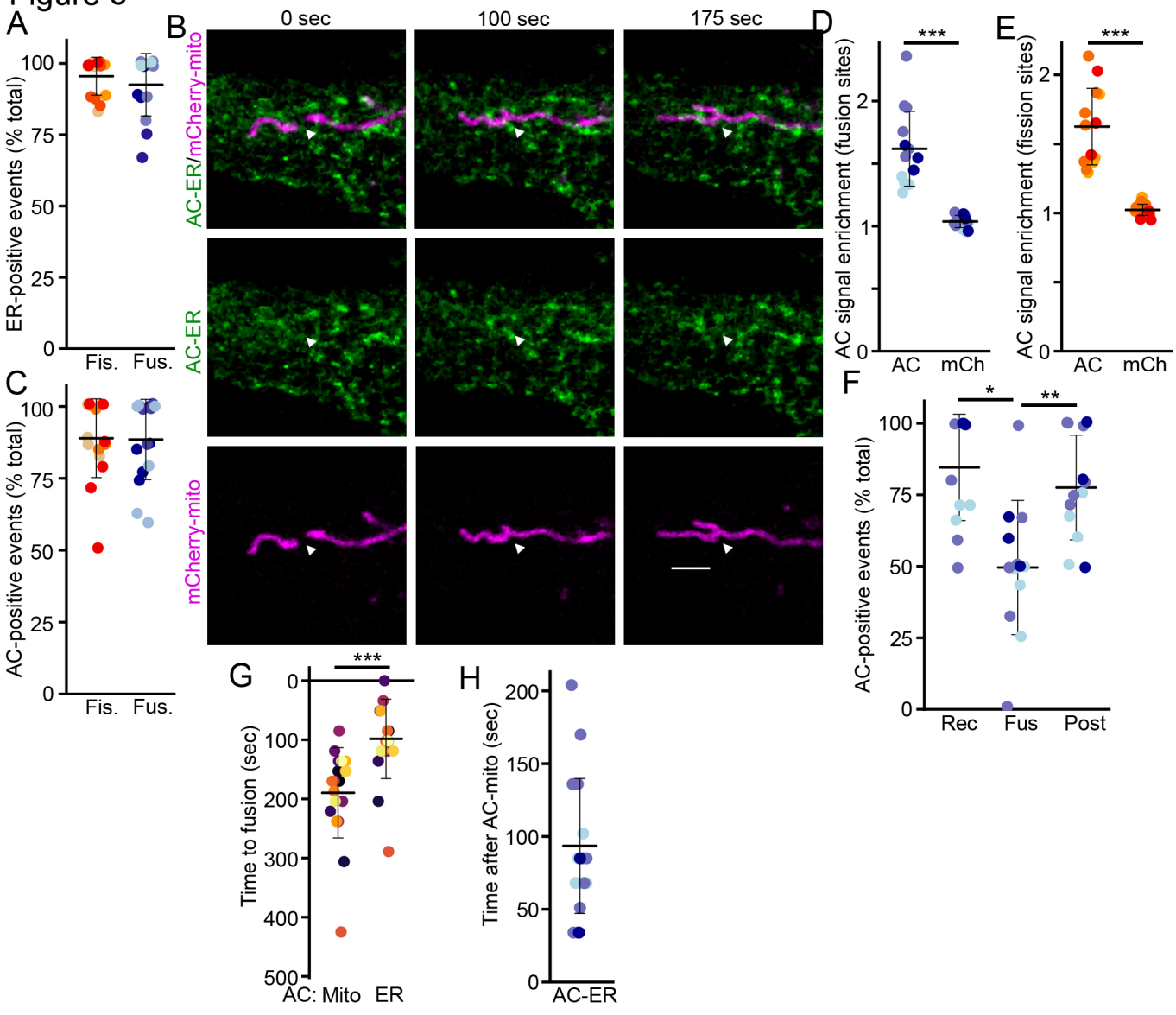

Figure 4

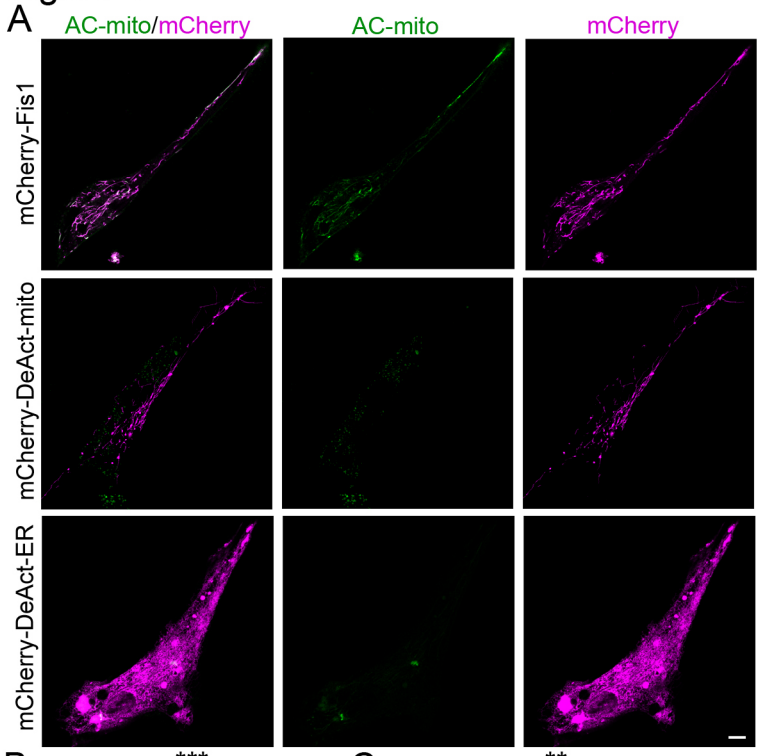

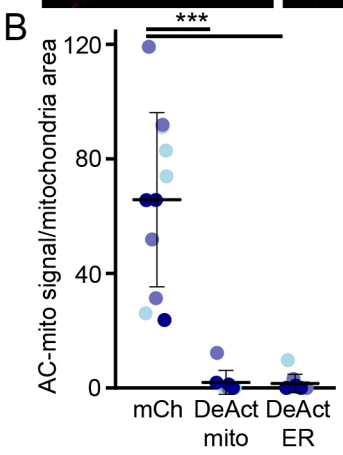

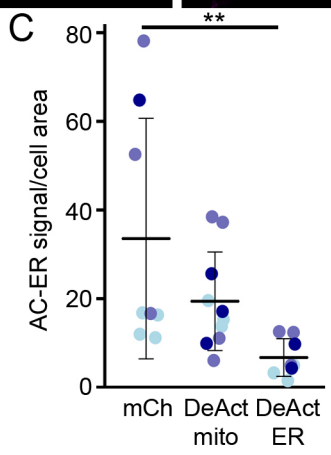

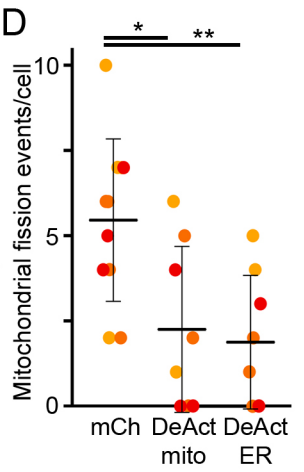

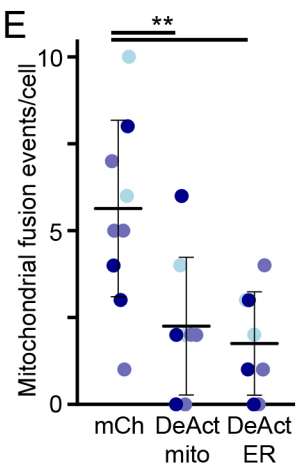

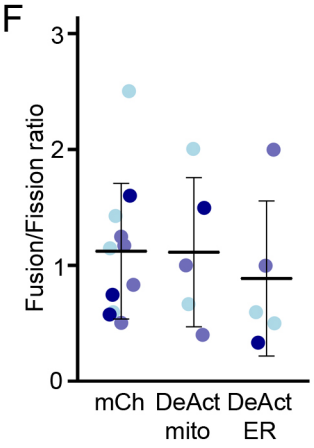

G

Type	mCh	DeAct-mito	DeAct-ER
End-to-End	11	10	9
End-to-Side	33	8	5
% Side	75%	44%	36%

Figure 5

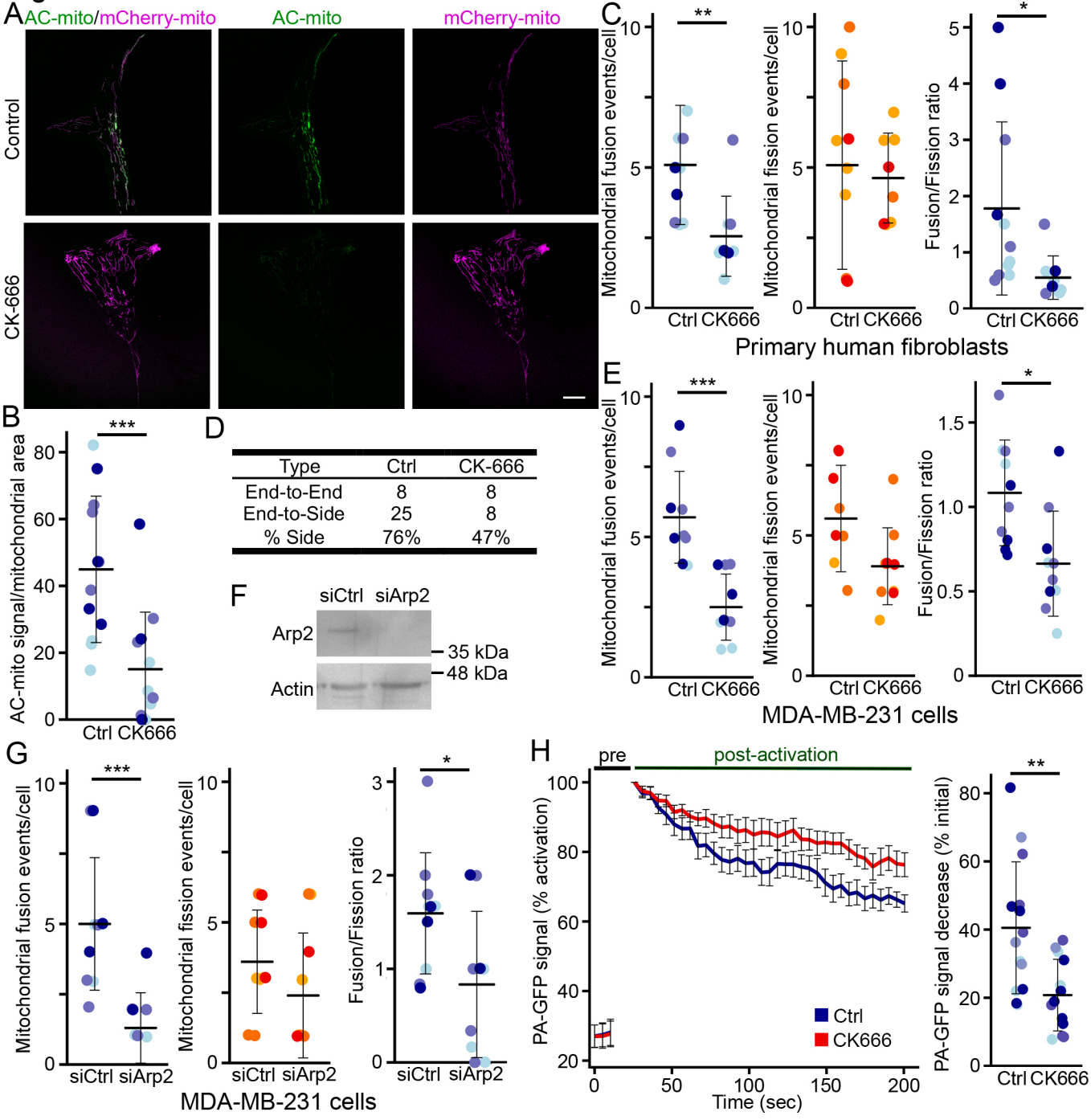

Figure 6

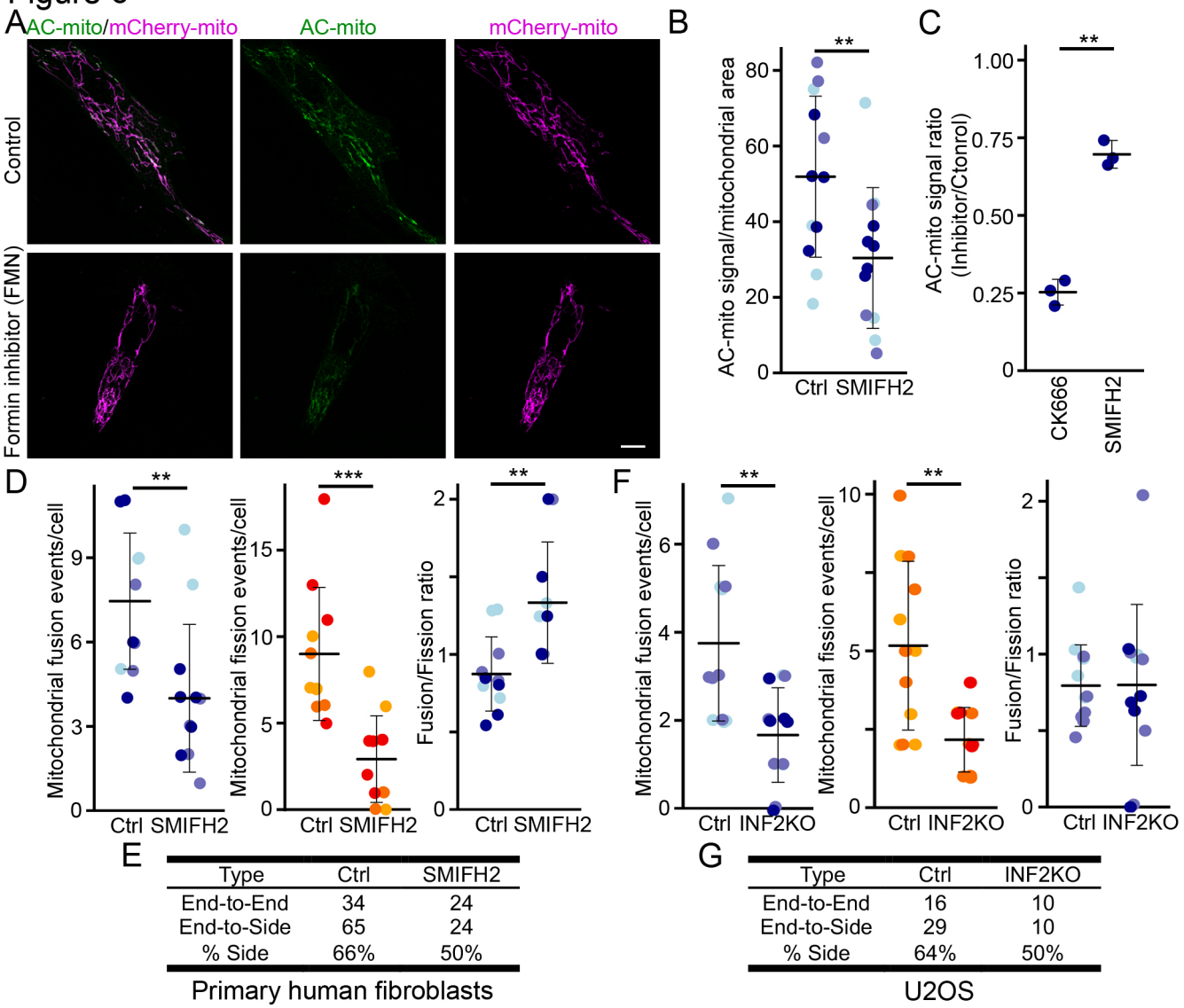

E

Type	Ctrl	SMIFH2
End-to-End	34	24
End-to-Side	65	24
% Side	66%	50%

Primary human fibroblasts

G

Type	Ctrl	INF2KO
End-to-End	16	10
End-to-Side	29	10
% Side	64%	50%

U2OS

Supplemental Figure 1

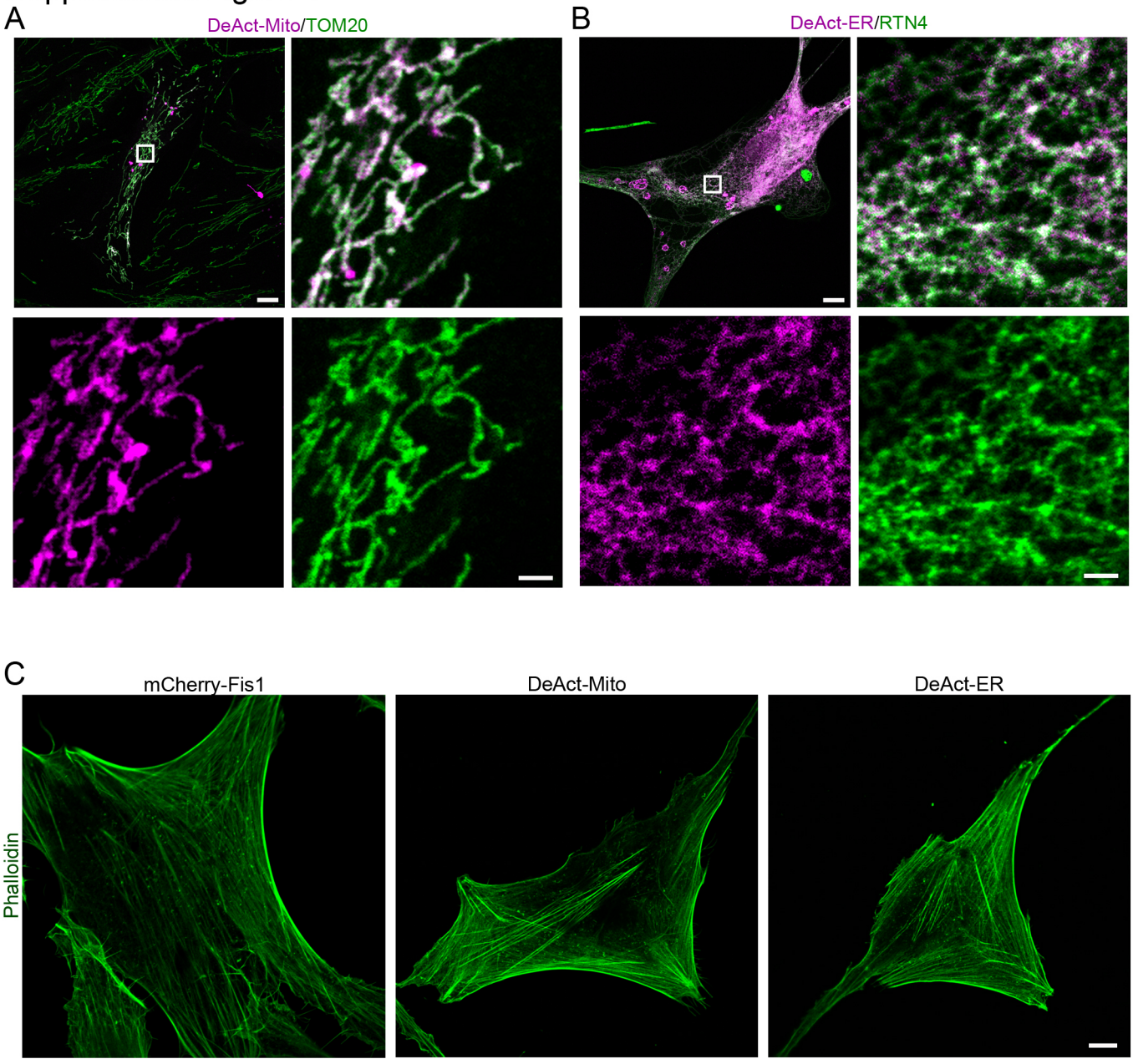

Supplemental Figure 2

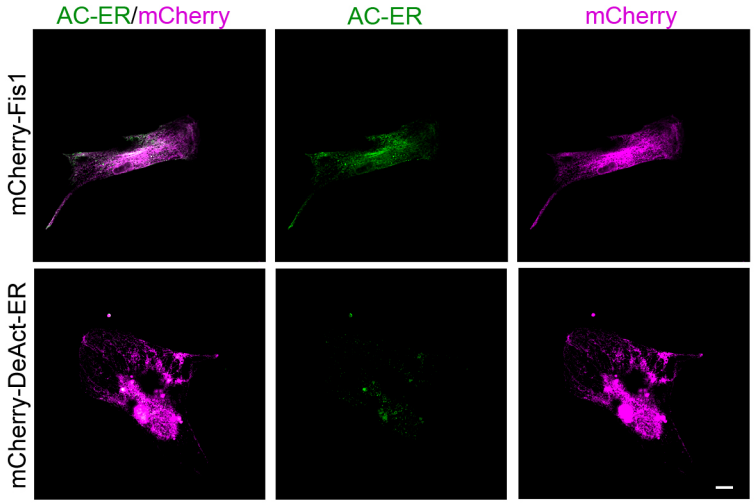

Supplemental Figure 3